Supplementary file for "High-fidelity, accelerated whole-brain submillimeter in-vivo diffusion MRI using gSlider-Spherical Ridgelets (gSlider-SR)

Gabriel Ramos-Llordén [*1], Lipeng Ning[1], Congyu Liao[2], Rinat Mukhometzianov[1,3], Oleg Michailovich[3], Kawin Setsompop[2], and Yogesh Rathi[1]

[1]Department of Psychiatry, Brigham and Women's Hospital, Harvard Medical School, Boston, Massachusetts, USA

[2]Athinoula A. Martinos Center for Biomedical Imaging, Massachusetts General Hospital, Harvard Medical School, Boston, Massachusetts, USA

[3]Department of Electrical and Computer Engineering, University of Waterloo, Waterloo, Ontario, Canada

Abstract

This supplementary files includes additional results that complement the content of the main paper. In particular, we include theoretical details of gSlider-SR in section 1, whereas additional results of the simulation and in-vivo experiments are presented in sections 2 and 3, respectively.

[*]**Corresponding author:**

Gabriel Ramos-Llordén

Psychiatry Neuroimaging Laboratory,

Department of Psychiatry,

Brigham and Women's Hospital, Harvard Medical School,

02215 Boston, Massachusetts, USA,

Telephone: +1 617-525-6124,

Email: gramosllorden@bwh.harvard.edu

1 gSlider-SR: theoretical aspects

1.1 Selection of the number of spherical ridgelets, M

The number of spherical ridgelets functions, M, is defined as $M = \sum_{j=-1}^{J} \left(2^{j+1} m_0 + 1\right)^2$, where J is the highest level of desired "resolution" and m_0 the minimum spherical order that fulfills a given error constraint (see construction of Spherical Ridgelets function in (1) for more details). We followed the recommendations of (1) and chose three resolution levels ($J = 1$) and $m_0 = 4$, giving a total of $M = 395$ SR basis functions. The multi-resolution and multi-frequency basis so obtained can represent any dMRI signal in the brain with high accuracy.

1.2 Analytical gradient formula w.r.t. phase maps of the Lagrangian cost-function, Eq.8

The gradient of cost-function Eq. 8 (in the main paper) w.r.t. $\boldsymbol{P}_k$ (with $L(\boldsymbol{P}_k)$ being the short-hand notation for the cost-function) can be calculated as (2):

$$\nabla L(\boldsymbol{P}_k) = 2\,\mathrm{Re}\{ie^{-i\boldsymbol{P}_k} \odot (\boldsymbol{D}_k \boldsymbol{S}\boldsymbol{\Omega}_k \odot \boldsymbol{M}^H(\boldsymbol{Y}_k - \boldsymbol{M}(e^{i\boldsymbol{P}_k} \odot \boldsymbol{D}_k \boldsymbol{S}\boldsymbol{\Omega}_k)) + \lambda_{phase}(e^{-i\boldsymbol{P}_k} \odot \boldsymbol{F}^H \boldsymbol{F} e^{i\boldsymbol{P}_k})\} \quad [S1]$$

where $\mathrm{Re}\{\cdot\}$ indicates the real part operator.

1.3 Convergence and computational complexity of gSlider-SR

It should be noted that the ADMM algorithm guarantees monotonic decrease of the cost-function of Eq. 6 even if the cost-function to be minimized is nonconvex (3) . Though we only iterate once in Eq. 8, that step guarantees a monotonically decrease, which does not compromise the overall convergence of the ADMM algorithm to a local minimum (at least). In cases where there is lack of proof for convergence to a global minimum, a common approach is to provide a reasonably well-chosen initialization (4). We adopted that approach, initializing gSlider-SR with a a Tikhonov regularization-based solution, providing satisfactory results both in simulated and in-vivo data experiments.

Computational complexity gSlider-SR was implemented in Matlab with some specific parts developed in C++, e.g.., the FISTA algorithm of Eq.9. This l_1 optimization problem is separable for every voxel, and was implemented to make use of multi-threading. For a super-resolution DWI

set with $N = 256 \times 256 \times 190$ voxels and $N_q = 64$ q-space points, and a mask considering brain-tissue only, the computation time was about $T_{l_1} = 15$ min in a computer with CPU: Intel Xeon Silver 4210 Processor with 20 cores at 2.2 GHz and 525 GB of RAM. Estimating $\boldsymbol{S}$ in Eq. 8 is a LLS problem that can be implemented very efficiently, about $T_{\boldsymbol{S}} = 10$ min in Matlab code. The most computationally demanding part was the non-linear estimation of thick-slice phase information $\boldsymbol{P}_k$ in Eq. 8. It took around $T_{\boldsymbol{P}_k} = 60$ min with a Matlab implementation of the NLCG method with Polak-Ribiere step. Solving the non-linear problem with quasi-Newton method would have perhaps converged faster, however, the memory requirements to estimate the Hessian would have rendered the problem infeasible. Total time of the gSlider-SR algorithm is then the number of iterations multiplied by $T_{\boldsymbol{S}} + T_{\boldsymbol{P}_k} + T_{l_1} = 85$ min. In the experiment section, we provide specific times for each experiment that is run with simulation and in-vivo data.

2 Simulation experiment

2.1 Mathematical details on the metrics used for validation

1. *Quality of signal reconstruction.* We used the following definition of NMSE

$$\text{NMSE} = \frac{||\hat{\boldsymbol{s}}_n - \boldsymbol{s}_n||_2^2}{||\boldsymbol{s}_n||_2^2}. \qquad \text{[S2]}$$

2. *Accuracy and precision in Fractional Anisotropy estimation.* To assess accuracy, we use the relative sample bias (or error), which is defined as

$$\frac{\overline{FA_e} - FA_{GT}}{FA_{GT}}, \qquad \text{[S3]}$$

where $\overline{FA_e}$ is the sample mean (over $MC = 20$ realizations) of FA_e, and FA_{GT} stands for the ground-truth FA. Precision is assessed by calculating the standard deviation of the $MC = 20$ realizations, $\text{std}(FA_e)$.

3. *Angular error in main diffusion tensor eigenvector.* The angular error (in degrees), Δ_θ, between the principal diffusion directions was computed (white matter region) as,

$$\Delta_\theta = \frac{180}{\pi} \arccos\left(\hat{\boldsymbol{u}} \cdot \boldsymbol{u}\right), \qquad \text{[S4]}$$

where $\hat{\boldsymbol{u}}$ is the main eigenvector of the tensor that is estimated from $\hat{\boldsymbol{S}}$ and $\boldsymbol{u}$ is that of the diffusion tensor estimated from $\boldsymbol{S}$.

4. *High Angular Reconstruction Diffusion Imaging (HARDI) results.*

   The principal diffusion directions and the number of fiber crossings (fiber peaks) were calculated. For a chosen peak in the ground-truth ODF, the angular error (in degrees) between the direction of that peak, $\boldsymbol{u}$, and the corresponding direction from the reconstructed ODF $\hat{\boldsymbol{u}}$, was calculated as in Eq. S4. Next, a single average angular error per voxel Δ_θ was computed by averaging all errors from each of the ODF peaks in that voxel.

2.2 DWI and diffusion-metrics maps for the four accelerated factors

Super-resolution DWI set and diffusion-metrics maps for acceleration factors: two, three, four and five are shown in Fig.1, Fig.2, Fig.3, and Fig.4, respectively.

3 In-vivo data experiment

3.1 Accounting for eddy-current and subject motion

The rationale behind the integrated affine registration step into gSlider-SR is the folllowing. Since the LLS problem for estimating $\boldsymbol{S}$ in Eq. 8 is separable along diffusion directions, the reconstruction of each high-resolution diffusion image is then free from motion artifacts. Nevertheless, the estimated DWI set $\boldsymbol{S}^{(t+1)}$ should be volume-wise registered before solving for Eq.9, as spherical-ridgelets fitting requires the DWI data to be aligned. Coefficients $\{\boldsymbol{c}_n^{(t+1)}\}_{n=1}^{N}$ are then estimated from a registered DWI dataset, $\mathcal{R}\{\boldsymbol{S}^{(t+1)}\}$, where registration is performed with the FSL tool `FLIRT` (5). Next, the synthetically generated image defined by $\boldsymbol{A}\boldsymbol{c}_n^{(t+1)}, n = 1, ..., N$, (third summand in Eq.8) is "unregistered" with the inverse transformation of $\mathcal{R}$, as the solution $\boldsymbol{S}$ in Eq. 8 is assumed to be affected by inter-volume motion, and voxel-wise correspondence is required. After iterating through this process, head motion and eddy-current distortion can be corrected using $\mathcal{R}\{\boldsymbol{S}^{(t_{\text{end}})}\}$ where t_{end} denotes the last iteration of the algorithm. The reference image for registration is the same b0 image that was used to account for eddy-current distortions and motion in the ground-truth dataset.

3.2 Estimated phase thick-slices maps

Estimated thick-slices phase maps with gSlider-SR are presented in Fig.5

References

1. Michailovich O, Rathi Y, Dolui S. Spatially regularized compressed sensing for high angular resolution diffusion imaging. *IEEE transactions on medical imaging* 2011; **30**(5):1100–15, doi:10.1109/TMI.2011.2142189. URL `http://www.ncbi.nlm.nih.gov/pubmed/21536524{%}0Ahttp://www.pubmedcentral.nih.gov/articlerender.fcgi?artid=PMC3708319`.

2. Zhao F, Noll DC, Nielsen JF, Fessler JA. Separate magnitude and phase regularization via compressed sensing. *IEEE transactions on medical imaging* 2012; **31**(9):1713–1723.

3. Ghadimi E, Teixeira A, Shames I, Johansson M. Optimal parameter selection for the alternating direction method of multipliers (admm): quadratic problems. *IEEE Transactions on Automatic Control* 2014; **60**(3):644–658.

4. Ning L, Setsompop K, Michailovich O, Makris N, Shenton ME, Westin CF, Rathi Y. A joint compressed-sensing and super-resolution approach for very high-resolution diffusion imaging. *NeuroImage* 2016; **125**:386–400, doi:10.1016/j.neuroimage.2015.10.061. URL `http://dx.doi.org/10.1016/j.neuroimage.2015.10.061`.

5. Jenkinson M, Bannister P, Brady M, Smith S. Improved optimization for the robust and accurate linear registration and motion correction of brain images. *NeuroImage* 2002; **17**(2):825 – 841, doi:https://doi.org/10.1006/nimg.2002.1132. URL `http://www.sciencedirect.com/science/article/pii/S1053811902911328`.

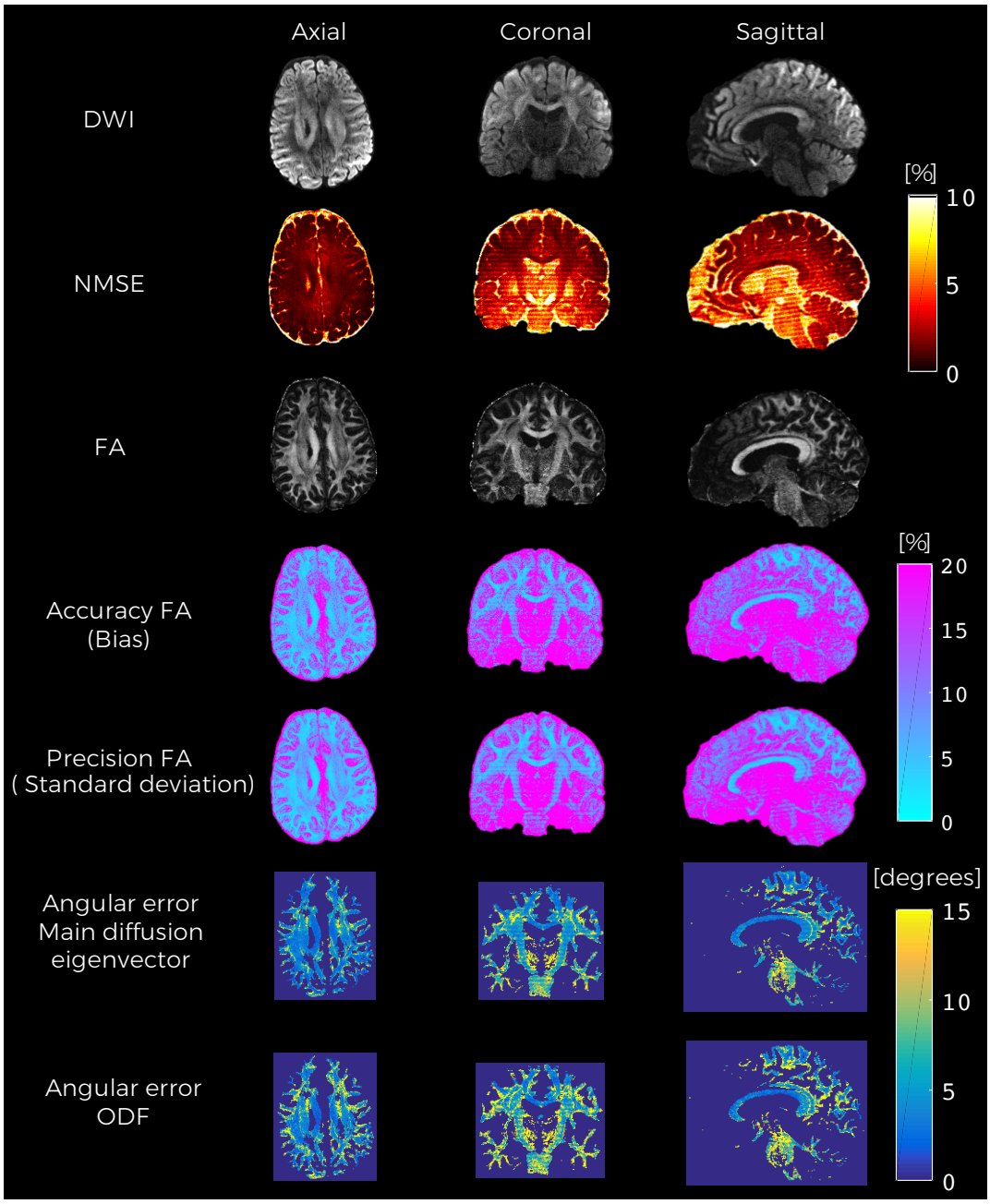

Figure 1: Reconstructed super-resolution DWI sets as well as diffusion-based metrics maps used in the simulation based experiment. Acceleration factor 2X.

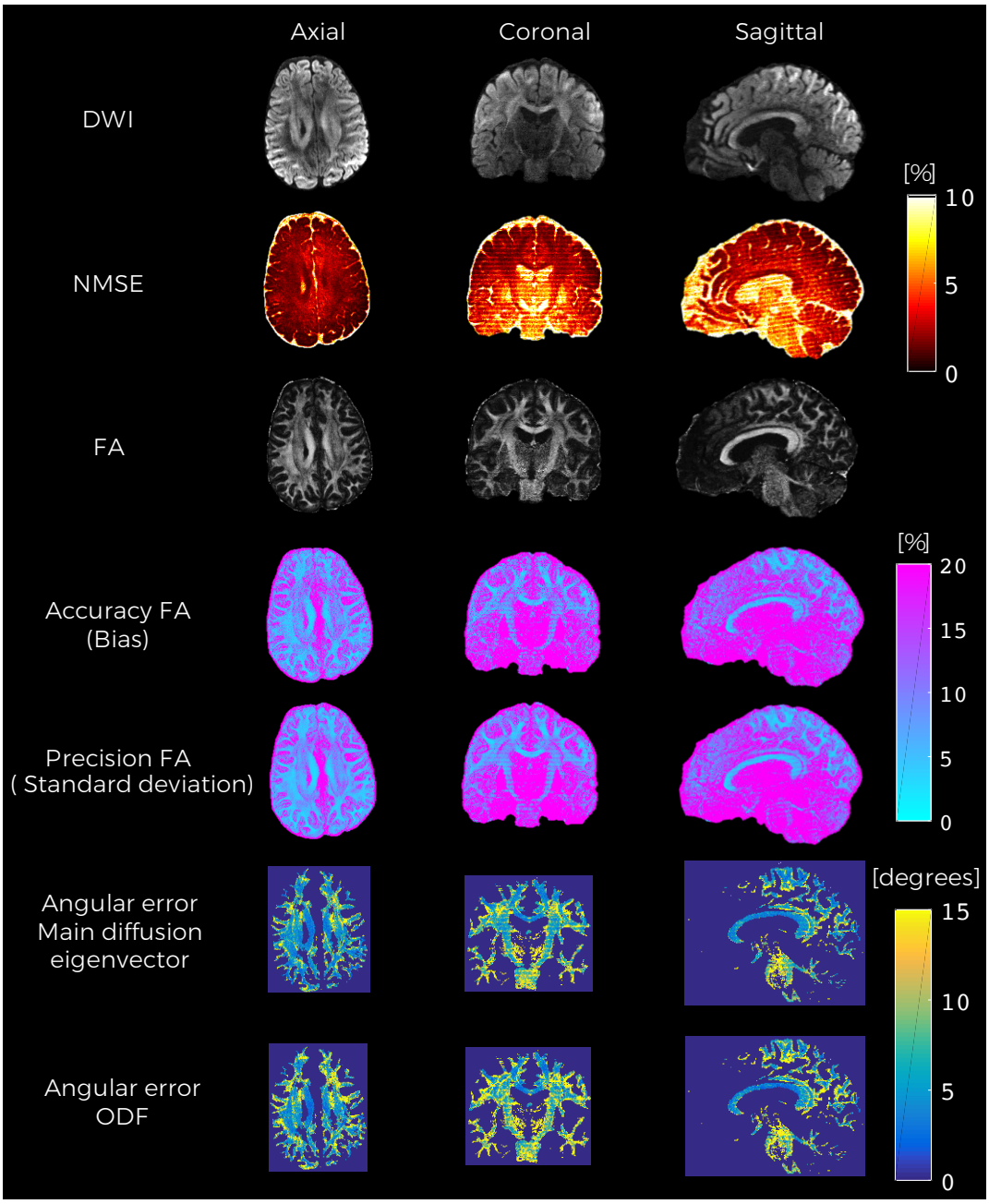

Figure 2: Reconstructed super-resolution DWI sets as well as diffusion-based metrics maps used in the simulation based experiment. Acceleration factor 3X.

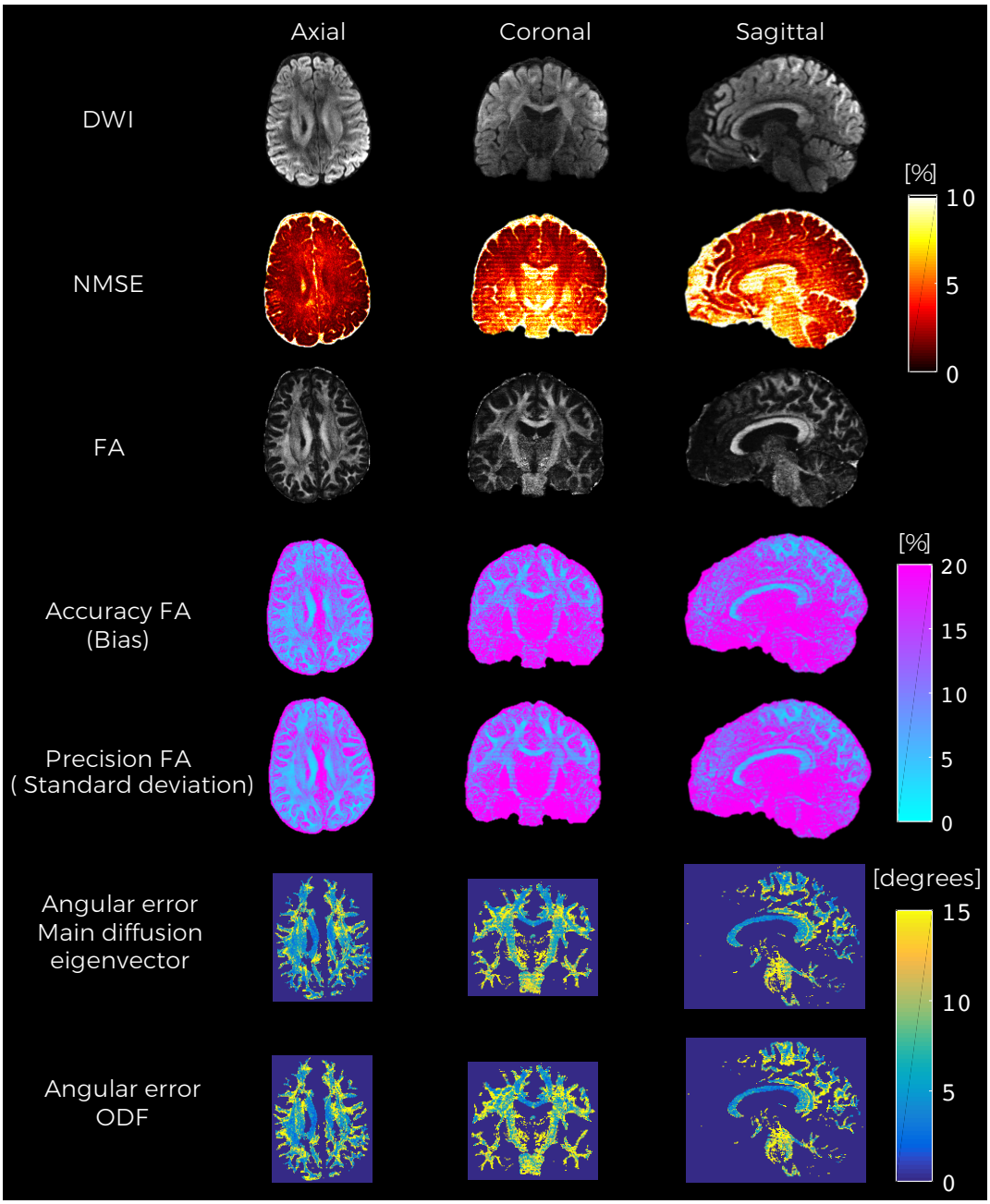

Figure 3: Reconstructed super-resolution DWI sets as well as diffusion-based metrics maps used in the simulation based experiment. Acceleration factor 4X.

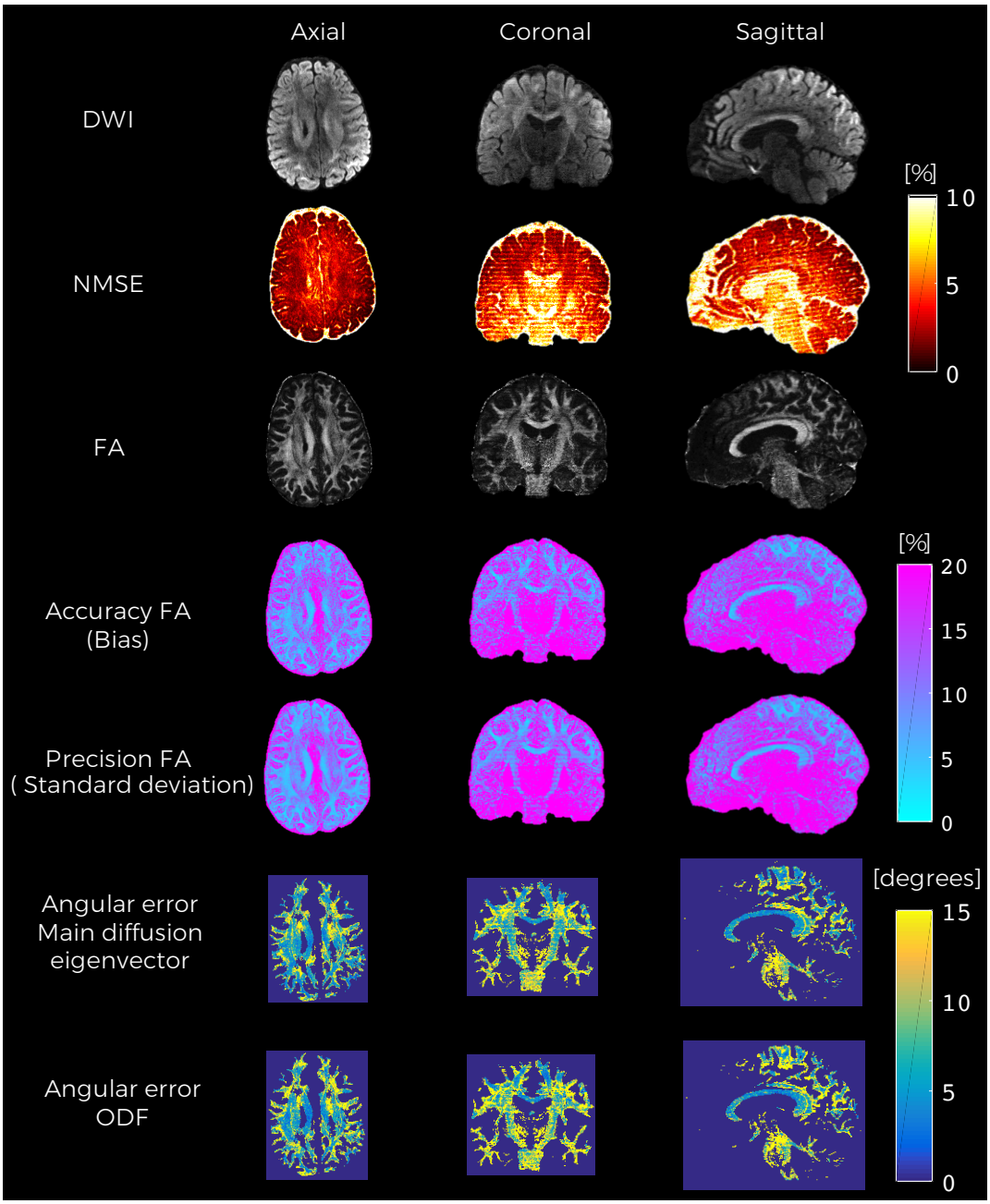

Figure 4: Reconstructed super-resolution DWI sets as well as diffusion-based metrics maps used in the simulation based experiment. Acceleration factor 5X.

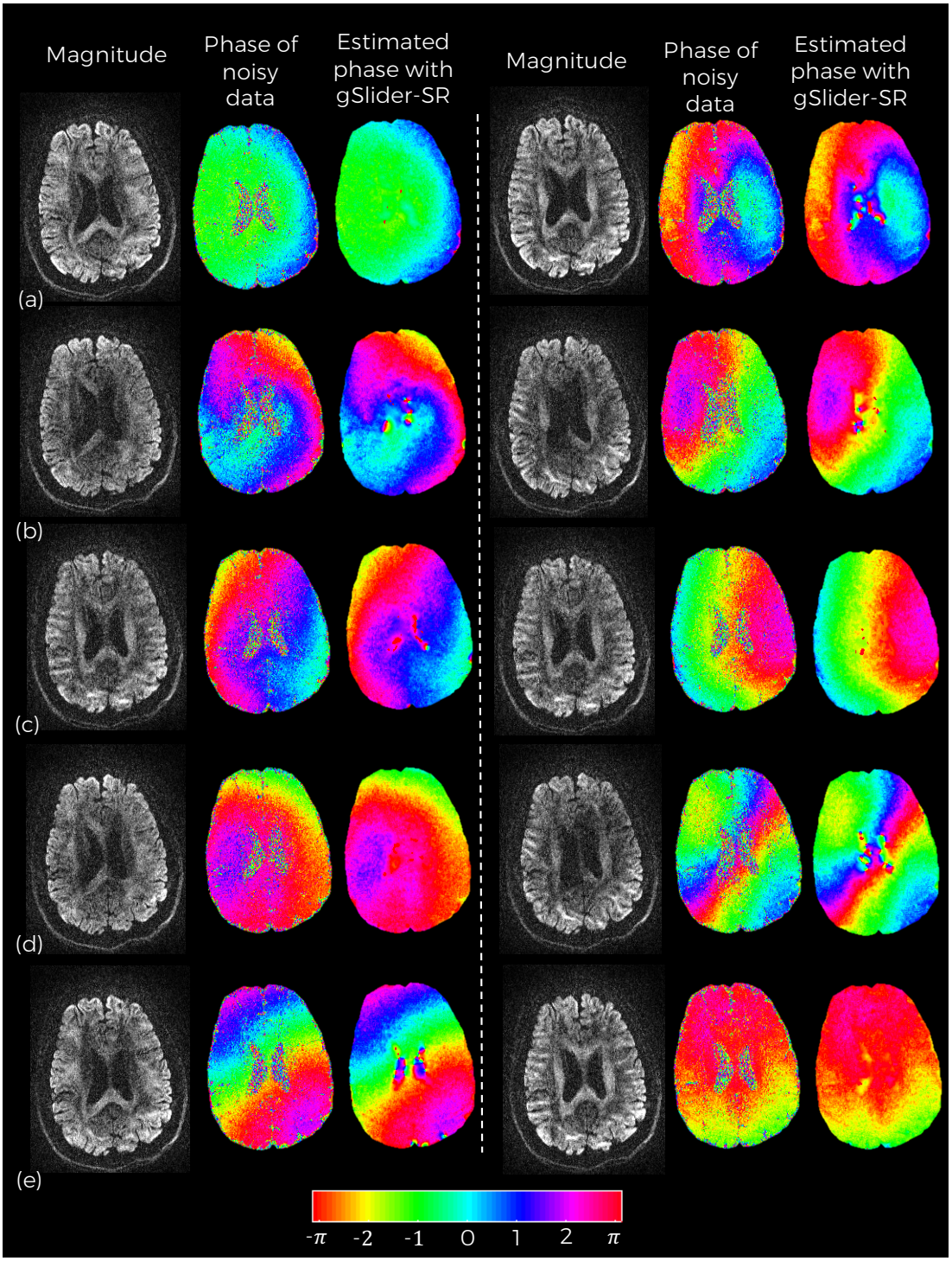

Figure 5: Estimated thick-slice phases map with gSlider-SR for two different gradient diffusion directions (left and right) and for the five RF-encoding profiles (a-e). Magnitude data as well as noisy phase thick slices are also shown.